

Inverse Compton X-ray Flare from GRB Reverse Shock

S. Kobayashi^{1,2,3}, B. Zhang⁴, P. Mészáros^{1,2} and D. Burrows²

ABSTRACT

We study synchrotron self-inverse Compton radiation from a reverse-shocked fireball. If the inverse Compton process dominates the cooling of shocked electrons, an X-ray flare produced by the first order Compton scattering would emerge in the very early afterglow phase, with the bulk of the shock energy radiated in the second order scattering component at 10-100 MeV. The dominance of inverse Compton cooling leads to the lack of prompt optical flashes. We show that for plausible parameters this scattering process can produce an X-ray flare with a relative amplitude change by a factor of several. Flares with a larger amplitude and multiple X-ray flares in a single event are likely to be produced by another mechanism (e.g. internal shocks).

Subject headings: gamma rays: bursts — shock waves — radiation mechanisms: nonthermal

1. Introduction

The Swift satellite is a multi-wavelength observatory designed to detect GRBs and their X-ray and UV/optical afterglows. Thanks to its fast pointing capabilities Swift is disclosing the early afterglow phase. The Swift X-Ray Telescope (XRT) found that most X-ray afterglows fall off rapidly for the first few hundred seconds, followed by a less rapid decline (Tagliaferri et al. 2005). In the early afterglows of GRB 050406 and GRB 050502b, XRT detected mysterious strong X-ray flares: rapid brightening of the X-ray afterglow after a few hundred seconds post-burst (Burrows et al. 2005). These results suggest the existence of additional emission components in the early afterglow phase besides the conventional forward shock emission.

¹Center for Gravitational Wave Physics, Pennsylvania State University, University Park, PA 16802

²Department of Astronomy and Astrophysics, Pennsylvania State University, University Park, PA 16802

³Astrophysics Research Institute, Liverpool John Moores University, Birkenhead CH41 1LD UK

⁴Department of Physics, University of Nevada, Las Vegas, NV 89154

In recent years, ground-based robotic telescopes reported the lack of prompt optical emission, except for a few cases. The Swift UV/Optical Telescope (UVOT) provided further stringent upper limits at very early epochs after the bursts (Roming et al. 2006). The limits ~ 20 mag at $\lesssim 100$ sec are much lower than the 9th magnitude optical flash associated with GRB 990123 (Akerlof et al. 1999). Although the host extinction at $z \sim 1$ and/or the high magnetization of a fireball (Zhang & Kobayashi 2005) can explain the lack of optical flashes, other suppression mechanisms might be involved.

According to the standard relativistic fireball model, reverse shocks are expected to radiate photons in the optical/IR band via the synchrotron process in a very early afterglow phase (Mészáros & Rees 1997; Sari & Piran 1999). Although the contribution of the reverse shock synchrotron emission to the X-ray band is small, electrons in the reverse-shocked region can up-scatter the synchrotron photons (synchrotron self-inverse Compton emission, hereafter SSC) to the X-ray or even higher energies ¹ (Mészáros & Rees 1993; Wang, Dai & Lu 2001a,b; Granot & Guetta 2003). The SSC emission should produce additional features in the early X-ray afterglows. If inverse-Compton (IC) cooling is the dominant cooling mechanism of the electrons, the energy available for the synchrotron process is significantly reduced, and prompt optical flashes could be faint (Beloborodov 2005). In this paper, we study the role of the reverse shock SSC emission in early X-ray afterglows.

2. Reverse Shocked Ejecta

We consider a relativistic shell (fireball ejecta) with an isotropic energy E and an initial Lorentz factor Γ_0 expanding into a homogeneous ambient medium with particle number density n . The evolution of reverse shocks is classified into two cases (Sari & Piran 1995) by using a critical Lorentz factor $\Gamma_c = (3(1+z)^3 E / 32\pi n m_p c^5 T^3)^{1/8} \sim 130 \zeta^{3/8} E_{52}^{1/8} T_2^{-3/8} n^{-1/8}$ where $\zeta = (1+z)/2$, $E_{52} = E/10^{52}$ ergs, $T_2 = T/10^2$ sec and T is the duration of the GRB. If $\Gamma_0 > \Gamma_c$ (thick shell case), the shell is significantly decelerated by a reverse shock. The Lorentz factor at the shock crossing time $t_d \sim T$ is given by $\Gamma_d \sim \Gamma_c$. If $\Gamma_0 < \Gamma_c$ (thin shell case), the reverse shock can not decelerate the shell effectively and $\Gamma_d \sim \Gamma_0$. The deceleration time $t_d = (1+z)(3E/32\pi\Gamma_0^8 n m_p c^5)^{1/3}$ is larger than the GRB duration.

We assume that constant fractions ϵ_e and ϵ_B of the shock energy go into the electrons and

¹Previous studies mainly address the prompt high-energy gamma-rays (> 100 MeV) detected by EGRET. Higher order scattering was ignored. As we will show, for plausible parameters the second order IC is important to discuss early afterglow. The correction significantly modifies the amplitude of an X-ray flare (the first order IC component) when the Compton parameter is large.

magnetic fields, respectively, and that electrons are accelerated in the shock to a power-law distribution $Nd\gamma \propto \gamma^{-p}d\gamma$, $\gamma \geq \gamma_m \sim [(p-2)/(p-1)]\epsilon_e(m_p/m_e)(\Gamma_0/\Gamma_d) \sim 180(\epsilon_e/0.3)(\Gamma_0/\Gamma_d)$ where $p = 2.5$ was assumed. Using the number of electrons in the shell N_e and the deceleration radius $R_d \sim 2c\Gamma_d^2 t_d/(1+z)$, the optical depth of the shell is $\tau(R_d) = \sigma_T N_e / 4\pi R_d^2 = (1/3)\mathcal{R}_M \sigma_T n R_d$ where we used the fact that the mass of the shell is larger by a factor of $\mathcal{R}_M = \Gamma_d^2/\Gamma_0$ than that of the ambient material swept by the shell at the deceleration time.

3. The First and Second order IC

Reverse-shocked electrons emit optical photons via the synchrotron process. Since the random Lorentz factors of electrons are typically a few hundreds, the up-scattered photons are in X-ray band. If the first order IC is in the X-ray band ($h\nu_X \sim 5$ keV), the comoving photon energy of the first IC is $h\nu'_X = h\nu_X/\Gamma \sim 50$ eV where Γ is the bulk Lorentz factor of the shocked shell. The Klein-Nishina effect does not suppress the second order IC scattering as long as the random Lorentz factor γ_m is below $\sim m_e c^2/h\nu'_X \sim 100\Gamma$. The second IC component appears in 10 – 100 MeV range. Higher order scattering (three or more) can be ignored because of the Klein-Nishina effect.

The ratio of the IC to synchrotron luminosity can be computed in a general way (Sari & Esin 2001). The luminosity ratios, in the limit of up to second scattering, are given by

$$x \equiv \frac{L_{IC,1st}}{L_{syn}} = \frac{U_{syn}}{U_B} = \eta \frac{U_e}{U_B} \left(1 + \frac{U_{IC,1st}}{U_{syn}} + \frac{U_{IC,2nd}}{U_{syn}} \right)^{-1} = \eta \frac{\epsilon_e}{\epsilon_B} (1 + x + x^2)^{-1} \quad (1)$$

$$x_2 \equiv \frac{L_{IC,2nd}}{L_{syn}} = \frac{U_{IC,1st}}{U_B} = \frac{U_{IC,1st}}{U_{syn}} \frac{U_{syn}}{U_B} = x^2 \quad (2)$$

where U_{syn} , $U_{IC,1st}$, $U_{IC,2nd}$, U_B and U_e are the energy density of synchrotron radiation, the 1st IC, 2nd IC, magnetic field and random electrons, respectively. We used $\eta U_e = U_{syn} + U_{IC,1st} + U_{IC,2nd}$. η is the fraction of the electron energy that was radiated away: $\eta = 1$ for fast cooling and $\eta = (\gamma_c/\gamma_m)^{2-p}$ for slow cooling. Solving eq (1) for x we obtain

$$x = \begin{cases} (\eta\epsilon_e/\epsilon_B) & \text{if } (\eta\epsilon_e/\epsilon_B) \ll 1 \\ (\eta\epsilon_e/\epsilon_B)^{1/3} & \text{if } (\eta\epsilon_e/\epsilon_B) \gg 1 \end{cases} \quad (3)$$

When the IC emission dominates the overall electron cooling, it reduces the energy available for synchrotron radiation. Consequently, the cooling-break energy of the electron distribution γ_c is reduced from the synchrotron-only value $\gamma_{c,s}$ by a factor of $(1 + x + x^2)$.

If $(\epsilon_e/\epsilon_B) \gg 1$ and $\eta_s \equiv (\gamma_{c,s}/\gamma_m)^{2-p} \ll 1$, the efficiency η depends on x . From eq. (1), one obtains $x \sim (\eta_s \epsilon_e/\epsilon_B)$ for $(\epsilon_e/\epsilon_B) < r_1$, $x \sim (\eta_s \epsilon_e/\epsilon_B)^{1/(7-2p)}$ for $r_1 < (\epsilon_e/\epsilon_B) < r_2$, and

$x \sim (\epsilon_e/\epsilon_B)^{1/3}$ for $(\epsilon_e/\epsilon_B) > r_2$ where $r_1 = \eta_s^{-1}$ and $r_2 = \eta_s^{-3/(2p-4)}$. A smaller ϵ_B makes the Compton parameter x larger, but the dependence is rather weak. Considering scalings $\eta_s \propto \epsilon_B^{p-2}$, $r_1 \propto \epsilon_B^{2-p} \sim \epsilon_B^{-1/2}$ and $r_2 \propto \epsilon_B^{-3/2}$, the second regime $r_1 < (\epsilon_e/\epsilon_B) < r_2$ should be achieved in the limit of $\epsilon_B \rightarrow 0$. Then, we obtain $x \propto \epsilon_B^{-(3-p)/(7-2p)} \sim \epsilon_B^{-1/4}$ for $p = 2.5$.

4. SSC Emission from Reverse Shock

The synchrotron spectrum of reverse shock emission can be approximated by a broken power-law with break frequencies, typical frequency ν_m and cooling frequency ν_c (e.g. Sari, Piran & Narayan 1998). The 1st IC spectrum is also roughly described by a broken power law with break frequencies ν_m^{IC} and ν_c^{IC} . The spectral characteristics of the 1st SSC emission are given by

$$\nu_m^{IC} \sim 2\gamma_m^2 \nu_m, \quad \nu_c^{IC} \sim 2\gamma_c^2 \nu_c, \quad F_{max}^{IC} \sim \kappa \tau F_{max}, \quad (4)$$

where κ is a correction coefficient. The ratio of νF_ν peaks also gives their luminosity ratio. It is $L_{IC,1st}/L_{syn} \sim \nu F_\nu^{IC}(\nu_{peak}^{IC})/\nu F_\nu(\nu_{peak}) = 2\kappa \tau \gamma_m \gamma_c \eta$ where $\nu_{peak} = \max[\nu_m, \nu_c]$ and $\nu_{peak}^{IC} = \max[\nu_m^{IC}, \nu_c^{IC}]$. We can reduce this estimate to eq. (3) with a normalization $\kappa = 4(p-1)/(p-2)$.

To assess the relative importance of the 1st IC emission and the synchrotron emission in the X-ray band (the 2nd IC component is well above X-ray band), we consider the flux ratio at the IC (F_ν) peak. For slow cooling, the IC spectrum peaks at ν_m^{IC} , and declines as $F_\nu^{IC} \propto \nu^{-(p-1)/2}$ for $\nu_m^{IC} < \nu < \nu_c^{IC}$ and as $F_\nu^{IC} \propto \nu^{-p/2}$ above ν_c^{IC} , while the synchrotron spectrum peaks at ν_m , and declines as $F_\nu \propto \nu^{-(p-1)/2}$ for $\nu_m < \nu < \nu_c$ and as $F_\nu \propto \nu^{-p/2}$ above ν_c . The flux ratio at the F_ν^{IC} peak is given by

$$\frac{F_\nu^{IC}(\nu_m^{IC})}{F_\nu(\nu_m^{IC})} = \frac{F_{max}^{IC}}{F_\nu(\nu_m^{IC})} \lesssim \gamma_m^{p-2} x \quad (5)$$

where $p < 3$ was assumed. The effective Compton parameter $x = 2\kappa \tau \gamma_m \gamma_c \eta$; the equality is achieved only when $\nu_c \sim \nu_m$. If electrons are in the fast cooling regime, the 1st IC peaks at ν_c^{IC} . We can show that the flux ratio at ν_c^{IC} has the same upper limit $\lesssim \gamma_m^{p-2} x$. Therefore, the contrast of a SSC bump should be less than $\gamma_m^{p-2} x \sim 10x (\epsilon_e/0.3)^{p-2} (\Gamma_0/\Gamma_d)^{p-2}$ where $(\Gamma_0/\Gamma_d) \sim 1$ for a thin shell. The bump could be more significant in the thick shell case, but in this case the SSC emission occurs at the end of the prompt gamma-ray emission, and it is difficult to separate the SSC emission from the internal shock signal.

If the ϵ_B parameter is small, the IC cooling becomes more important compared to the synchrotron cooling. However, as we showed at the end of the previous section, the dependence is weak: $x \propto \epsilon_B^{-1/4}$. To achieve $x \gg 1$, a very small ϵ_B is required. The cooling

frequency ν_c then becomes much higher than the typical frequency ν_m . It is possible to show that the flux ratio at ν_m^{IC} is insensitive to ϵ_B as $F_\nu^{IC}(\nu_m^{IC})/F_\nu(\nu_m^{IC}) = (F_{max}^{IC}/F_{max})(\nu_m^{IC}/\nu_m)^{(p-1)/2} \sim x\gamma_c^{p-3} \propto \epsilon_B^0$. For plausible parameters, x could be several at most. If x is large, most energy is radiated in the 2nd IC component, the SSC bump and the base line X-ray afterglow should be faint. The synchrotron emission (optical flash) should be highly suppressed.

5. Forward Shock Emission

A forward shock also emits X-rays via the synchrotron process. At the deceleration time, the spectral characteristics of the forward and reverse shock synchrotron emission are related (e.g. Zhang, Kobayashi & Mészáros 2003) as

$$\nu_{m,f} \sim \mathcal{R}_B^{1/2} \mathcal{R}_M^2 \nu_m, \quad \nu_{c,f} \sim \mathcal{R}_B^{-3/2} \mathcal{R}_X^{-2} \nu_c, \quad F_{max,f} \sim \mathcal{R}_B^{1/2} \mathcal{R}_M^{-1} F_{max} \quad (6)$$

where the subscript f denotes forward shock quantities, we have assumed that the ϵ_e and p parameters are the same for both shock regions, but with different ϵ_B as parameterized by $\mathcal{R}_B = (\epsilon_{B,f}/\epsilon_B)$. The reason we introduce the \mathcal{R}_B parameter is that the fireball ejecta could be endowed with a primordial magnetic field (e.g. Zhang et al. 2003 and references therein). $\mathcal{R}_X = (1 + x_f)/(1 + x + x^2)$ is a correction factor for the IC cooling. In the forward shock region, a once-scattered synchrotron photon generally has energy larger than the electron mass in the rest frame of the second scattering electrons. Multiple scattering of synchrotron photons can be ignored. We obtain $x_f = (\eta\epsilon_e/\epsilon_{B,f})$ for $(\eta\epsilon_e/\epsilon_{B,f}) \ll 1$ and $x_f = (\eta\epsilon_e/\epsilon_{B,f})^{1/2}$ for $(\eta\epsilon_e/\epsilon_{B,f}) \gg 1$ (Sari & Esin 2001). $\mathcal{R}_M = \Gamma_d^2/\Gamma_0$ is the mass ratio defined in section 2.

The 1st IC peak is much lower than that of the forward shock as $F_{max}^{IC}/F_{max,f} \lesssim 2 \times 10^{-4} \mathcal{R}_B^{-1/2} n \Gamma_{0,2} R_{d,17}$. Since the typical frequencies $\nu_{m,f}$ and ν_m^{IC} are around the X-ray band in the early afterglow phase, the forward shock emission should peak at a low cooling frequency $\nu_{c,f} \ll \nu_X$ (this could be achieved with a moderate density ambient medium), otherwise the SSC emission is masked by the forward shock emission.

6. Light Curves of SSC emission

After a reverse shock crosses the shell, the hydrodynamic quantities of a fluid element in the shell evolves as the Lorentz factor $\Gamma \propto R^{-7/2}$, the mass density $\rho \propto R^{-3}\Gamma$ and the internal energy $e \propto \rho^{4/3}$ for a thick shell case, while for a thin shell case they can be approximated as $\Gamma \propto R^{-2}$, $\rho \propto (R^{-3}\Gamma)^{6/7}$ and $e \propto \rho^{4/3}$ (Kobayashi & Sari 2000). Using these scalings, one obtains that the flux below the peak frequency $\min[\nu_m^{IC}, \nu_c^{IC}]$ evolves as $\sim t^{-1/2}$ for a thick shell and $\sim t^{-2/3}$ for a thin shell. The flux between ν_m^{IC} and ν_c^{IC} falls as $\sim t^{-(5p+1)/5}$

for a thick shell and $\sim t^{-(3p+1)/3}$ for a thin shell. When $\nu_c^{IC} \sim t^{-2}$ becomes lower than the observed frequency, the flux drops exponentially with time. However, the angular time delay effect prevents an abrupt disappearance. The flux will be determined by off-axis emission if the line-of-sight emission decays faster than $t^{-2+\beta}$ where $\beta = -(p-1)/2$ or $-p/2$ is the spectral index (Kumar & Panaiteescu 2000).

The temporal index of a SSC flare in the rising phase is rather uncertain, because it depends on the density profile of the fireball shell. We assume a simple homogeneous shell. The hydrodynamic quantities and the number of shocked electrons during shock crossing are given by $\Gamma \propto R^{-1/2}$, $e \propto \Gamma^2$, $\rho \propto R^{-2}\Gamma^{-1}$ and $N_e \propto R^2$ for a thick shell, and $\Gamma \propto R^{-g}$, $e \propto \Gamma^2$ and $\rho \propto R^{-3}\Gamma^{-1}$ and $N_e \propto R^{3/2}$ for a thin shell where g is a parameter (e.g. Kobayashi 2000). Around the shock crossing, the shock becomes mildly relativistic (Sari & Piran 1995; Kobayashi, Piran & Sari 1999). We consider the behavior of a light curve near the peak ($g = 1/2$). The break frequencies of the SSC emission evolve as $\nu_c^{IC} \propto t^{-3/2}$, $\nu_m^{IC} \propto t^{1/2}$ (thick shell) or $t^{5/2}$ (thin shell). Since during the shock crossing ν_m^{IC} increases while ν_c^{IC} decreases, an interesting regime is $\nu_m^{IC} < \nu_{obs} < \nu_c^{IC}$. Assuming $p = 2.5$, for a thick shell the flux increases as $t^{7/8}$ in this regime, and it is almost constant in the other regimes. For a thin shell, the flux in this regime increases as $t^{15/8}$. If ν_m^{IC} (or ν_c^{IC}) crosses ν_{obs} , the flux behaves as $t^{-5/6}$ (or $t^{9/8}$). If both break frequencies pass the observed frequency $\nu_c^{IC} < \nu_{obs} < \nu_m^{IC}$, the flux decays as $t^{-3/4}$.

7. X-ray Flare from Thin Shell

In this section, we first study the typical thin shell case, and show the spectrum and light curve of the early afterglow. If the reverse shock is in the thin shell regime, the SSC peak is separated from the GRB emission. The deceleration time is $t_d \sim 190 \zeta E_{52}^{1/3} (\Gamma_0/80)^{-8/3} (n/5)^{-1/3}$ sec. The typical and cooling frequencies of the forward shock synchrotron emission at the deceleration time are given (e.g. Sari, Piran & Narayan 1998) by

$$\nu_{m,f} \sim 7.0 \times 10^{16} \zeta^{-1} \left(\frac{\epsilon_{B,f}}{0.01} \right)^{1/2} \left(\frac{\epsilon_e}{0.3} \right)^2 \left(\frac{\Gamma}{80} \right)^4 \left(\frac{n}{5} \right)^{1/2} \text{ Hz}, \quad (7)$$

$$\nu_{c,f} \sim 1.9 \times 10^{14} \zeta^{-1} E_{52}^{-2/3} \left(\frac{1+x_f}{6.5} \right)^{-2} \left(\frac{\epsilon_{B,f}}{0.01} \right)^{-3/2} \left(\frac{\Gamma}{80} \right)^{4/3} \left(\frac{n}{5} \right)^{-5/6} \text{ Hz}, \quad (8)$$

Using eq. (6), the break frequencies of the reverse shock synchrotron emission are

$$\nu_m \sim 1.9 \times 10^{13} \zeta^{-1} \left(\frac{\epsilon_B}{0.03} \right)^{1/2} \left(\frac{\epsilon_e}{0.3} \right)^2 \left(\frac{\Gamma}{80} \right)^2 \left(\frac{n}{5} \right)^{1/2} \text{ Hz}, \quad (9)$$

$$\nu_c \sim 3.9 \times 10^{13} \zeta^{-1} E_{52}^{-2/3} \left(\frac{1+x+x^2}{6.2} \right)^{-2} \left(\frac{\epsilon_B}{0.03} \right)^{-3/2} \left(\frac{\Gamma}{80} \right)^{4/3} \left(\frac{n}{5} \right)^{-5/6} \text{ Hz}, \quad (10)$$

where we assumed a larger value of ϵ_B for the fireball than that of the blast wave. Using eq. (4), the break frequencies of the reverse shock SSC emission are

$$\nu_m^{IC} \sim 1.2 \times 10^{18} \zeta^{-1} \left(\frac{\epsilon_B}{0.03} \right)^{1/2} \left(\frac{\epsilon_e}{0.3} \right)^4 \left(\frac{\Gamma}{80} \right)^2 \left(\frac{n}{5} \right)^{1/2} \text{ Hz}, \quad (11)$$

$$\nu_c^{IC} \sim 5.3 \times 10^{18} \zeta^{-1} E_{52}^{-4/3} \left(\frac{1+x+x^2}{6.2} \right)^{-4} \left(\frac{\epsilon_B}{0.03} \right)^{-7/2} \left(\frac{\Gamma}{80} \right)^{2/3} \left(\frac{n}{5} \right)^{-13/6} \text{ Hz} \quad (12)$$

We plot the broad band spectrum in figure 1. The reverse shock SSC emission (thick solid line) dominates X-ray band ($5\text{keV} \sim 10^{18} \text{ Hz}$) in this example case. Figure 2 shows an X-ray light curve around the deceleration time. The reverse shock SSC emission produces an X-ray flare around the deceleration time. For reference, we plot the X-ray light curve of GRB 050406. Compared to the theoretical SSC flare (thick solid line), the observed flare rises more rapidly, especially around the peak. As we gave a caveat in the previous section, the temporal index in the rising phase is rather uncertain. This sharp rise might be due to inhomogeneity of a fireball shell (we have assumed a homogeneous shell to evaluate the light curve). The internal shock model requires a highly irregular outflow from the GRB central engine. Since the hydrodynamic interaction inside the flow smooths the velocity and pressure profiles, but not the density profile, fireball ejecta might have an irregular density profile at the deceleration time. Emission from the ejecta during a reverse shock crossing could reflect the light curve of the prompt emission produced by internal shocks (Nakar & Piran 2004). The duration of GRB 050406 was $T_{90} = 5 \pm 1 \text{ s}$ in the 15-350keV band and the light curve peak had a fast rise, exponential decay (FRED) profile (Krimm et al. 2005). Around the peak, a reverse shock might hit a higher density part of the shell.

Another possibility is that a reverse shock might stay in the Newtonian regime during the whole evolution. The SSC emission from a Newtonian reverse shock is expected to rise as rapidly as $\propto t^{4p-2} = t^8$ for $p = 2.5$ (thick dashed line). In such a case, the forward shock emission also increases faster (thin dashed line). This could happen if later ejecta from the central engine injects additional energy to the inner tail of the shell after the internal shock phase, and it further smooths the velocity profile of the shell. When the spreading of a shell width is not significant, a reverse shock does not evolve to mildly relativistic at the deceleration time (Sari & Piran 1995). X-ray flares with a moderate amplitude like this event can be produced by the reverse shock SSC process, although the sharp structure $dt/t < 1$ might be difficult to be explained in external shock related models (Kobayashi & Zhang 2006).

We consider how the relative amplitude of X-ray flares depends on parameters. Since

X-ray flares occur a few hundred seconds after the prompt emission, we will consider the thin shell case. Fixing the deceleration time $t_d \sim 190 \zeta E_{52}^{1/3} (\Gamma_0/80)^{-8/3} (n/5)^{-1/3}$ sec, the initial Lorentz factor is a function of the ISM density (we assume the typical explosion energy and redshift). A larger ratio of ϵ_e/ϵ_B enhances the scattering process. Assuming the equipartition value $\epsilon_e = 0.3$, we evaluate the relative amplitude of an X-ray flare as a function of ϵ_B . The results are shown for different values of n in figure 3. The amplitude is as large as a few tens if $\epsilon_B \ll 1$ and $n \gg 1$. However, a high density requires a low Lorentz factor (i.e. $\Gamma \sim 55$ for $n = 100$).

8. Conclusions

We have investigated the synchrotron self inverse-Compton (SSC) emission from the reverse shock. The synchrotron process is expected to produce optical/IR photons, which are up-scattered into the X-ray band by electrons heated by the reverse shock. For a thick shell, the X-ray flare occurs at the end of the prompt gamma-ray phase. The emission decays as $\sim t^{-2}$ or slightly steeper. For a thin shell, the emission initially increases as $\sim t^2$ (the scaling could be significantly different if a fireball shell is highly irregular), the peak should be separated from the prompt emission, and after the peak the flux decays as $\sim t^{-(3p+1)/3}$ or steeper. If off-axis radiation dominates, the temporal and spectral indices $L \propto t^\alpha \nu^\beta$ should satisfy the relation $\alpha = -2 + \beta$. A weakly magnetized fireball ($\epsilon_{B,f} < \epsilon_B \ll 1$) in a high density ambient medium provides favorable conditions for producing a significant X-ray flare. The contrast between the IC flare and the baseline X-ray emission is at most one order of magnitude if the synchrotron process dominates the electron cooling. If the IC dominates, the contrast could be larger. However, since most of the energy is radiated in the 2nd order IC component around 10-100 MeV, the X-ray bump and the baseline X-ray emission are less energetic than the latter. The optical flash (due to synchrotron) is highly suppressed.

Recently Swift XRT detected X-ray flares in the early afterglows of GRB 050406 and GRB 050502b (Burrows et al 2005). The afterglow of GRB 050406 brightens by a factor of 6 between 100 and 200 s post-burst before starting on the rapid decline seen in other prompt X-ray afterglows. GRB 050502b had an even stronger X-ray flare, brightening by a factor of $\sim 10^3$ to a peak 700 s after the burst. Both afterglows were very faint at 100 s post-burst (a factor of a few - 100 fainter than previous XRT-detected afterglows).

In the case of GRB 050502b, the X-ray flare contrast factor $\sim 10^3$ requires a Compton parameter x larger than ~ 100 , which means $\epsilon_e/\epsilon_B \gtrsim 10^8$. With plausible values of the other parameters, the SSC emission should appear at an energy band well above X-rays. The very sharp profile $dt/t \ll 1$ also rules out external shock models. Another mechanism

(e.g late time internal shocks; Burrows et al. 2005; Falcone et al. 2006; Romano et al 2006; Zhang et al. 2006; Nousek et al. 2006; Fan & Wei 2005; Wu et al. 2005; Ioka, Kobayashi & Zhang 2005) is likely to play a role in the production of the X-ray flare. On the other hand, the X-ray flare of GRB 050406 might be explained with the reverse shock SSC emission discussed here, although the rather narrow feature $dt/t < 1$ might disfavor the external shock interpretation. If we apply the SSC model to the flare, the peak time $t_d \sim 200$ sec gives an initial Lorentz factor $\Gamma_0 \sim 80 (t_d/200\text{s})^{3/8} \zeta^{3/8} E_{52}^{1/8} (n/5)^{-1/8}$. The reverse shock SSC emission can not explain multiple X-ray flares in a single event. Such behavior is observed in recent Swift bursts (Burrows et al. 2005; Falcone et al. 2006; Romano et al. 2006; O’Brien et al. 2006).

In thick shell cases, the SSC flare rising portion overlaps in time with the prompt emission seen by BAT. Although it could be difficult to separate the X-ray emission of the prompt and the reverse SSC flare rising components, the rapidly decaying portion of the reverse SSC flare could be detectable. Swift has reported many of the X-ray afterglows detected have an early steep decay phase, before going into a more common shallow decay. In some of these cases, the early steep decay may be interpreted as the tail portion of a reverse shock SSC X-ray flare.

We note also that the reverse shock SSC mechanism predicts, besides an X-ray flare, a strong GeV flare from 2nd order IC, and in some cases from first order IC. Thus, bursts with strong early X-ray flares should be good candidates for GLAST.

We thank Patrizia Romano and the Swift team for providing XRT data. This work is supported by Eberly Research Funds of Penn State and by the Center for Gravitational Wave Physics funded by NSF under cooperative agreement PHY 01-14375 (for SK), NASA NNG04GD51G (for BZ), NASA AST 0098416 and NASA NAG5-13286 (for PM), and NASA Swift GI program (for BZ, SK and PM).

References

Akerlof,C.W. et al. 1999, *Nature*, 398, 400.

Beloborodov,A.M. 2005, *ApJ*, 618, L13.

Burrows,D. et al. 2005, *Science*, 309, 1833.

Falcone,A.D. et al. 2006, *ApJ*, 641, 1010.

Fan,Y. & Wei,D.M. 2005, *MNRAS*, 364, L42.

Granot,J.&Guetta,D. 2003, *ApJ*, 598, L11.

Ioka,K.,Kobayashi,S.& Zhang,B. 2005, *ApJ*, 631, 429.

Kobayashi,S 2000, *ApJ*, 545, 807.

Kobayashi,S, Piran,T. & Sari,R. 1999, *ApJ*, 513, 669.

Kobayashi,S & Sari,R. 2000, *ApJ*, 542, 819.

Kobayashi,S. & Zhang,B. 2006, submitted to *ApJ*, astro-ph/0608132.

Kumar,P. & Panaiteescu,A. 2000, *ApJ*, 541, L51.

Krimm,H. et al. 2005, *GCN* 3183

Mészáros ,P. & Rees,M.J. 1993, *ApJ*, 418, L59.

Mészáros,P. & Rees,M.J. 1997, *ApJ*, 476, 231.

Nakar,E. & Piran,T. 2004, *MNRAS*, 353, 647

Nousek,J.A. et al. 2006, *ApJ*, 642, 389.

O'Brien, P.T. et al. 2006, *ApJ*, 647, 1213.

Romano,P. et al. 2006 *A & A*, 450, 59.

Roming,.P et al. 2006 *ApJ* in press, astro-ph/0509273.

Sari,R. & Esin,A.A. 2001 *ApJ*, 548, 787.

Sari,R. & Piran,T. 1995 *ApJ*, 455, L143.

Sari,R. & Piran,T. 1999 *ApJ*, 520, 641.

Sari,R., Piran,T. & Narayan,R. 1998 *ApJ*, 497, L17.

Tagliaferri,G. et al. 2005 *Nature*, 436 985.

Wang,X.Y.,Dai,Z.G.&Lu,T. 2001a, ApJ, 546,L33.

Wang,X.Y.,Dai,Z.G.&Lu,T. 2001b, ApJ, 556, 1010.

Wu,X.F. et al. 2005, submitted to ApJ, astro-ph/0512555.

Zhang,B., Kobayashi,S. & Mészáros,P. 2003, ApJ, 595, 950.

Zhang,B. & Kobayashi,S. 2005, ApJ, 628, 315.

Zhang,B. et al. 2006, ApJ, 642, 354.

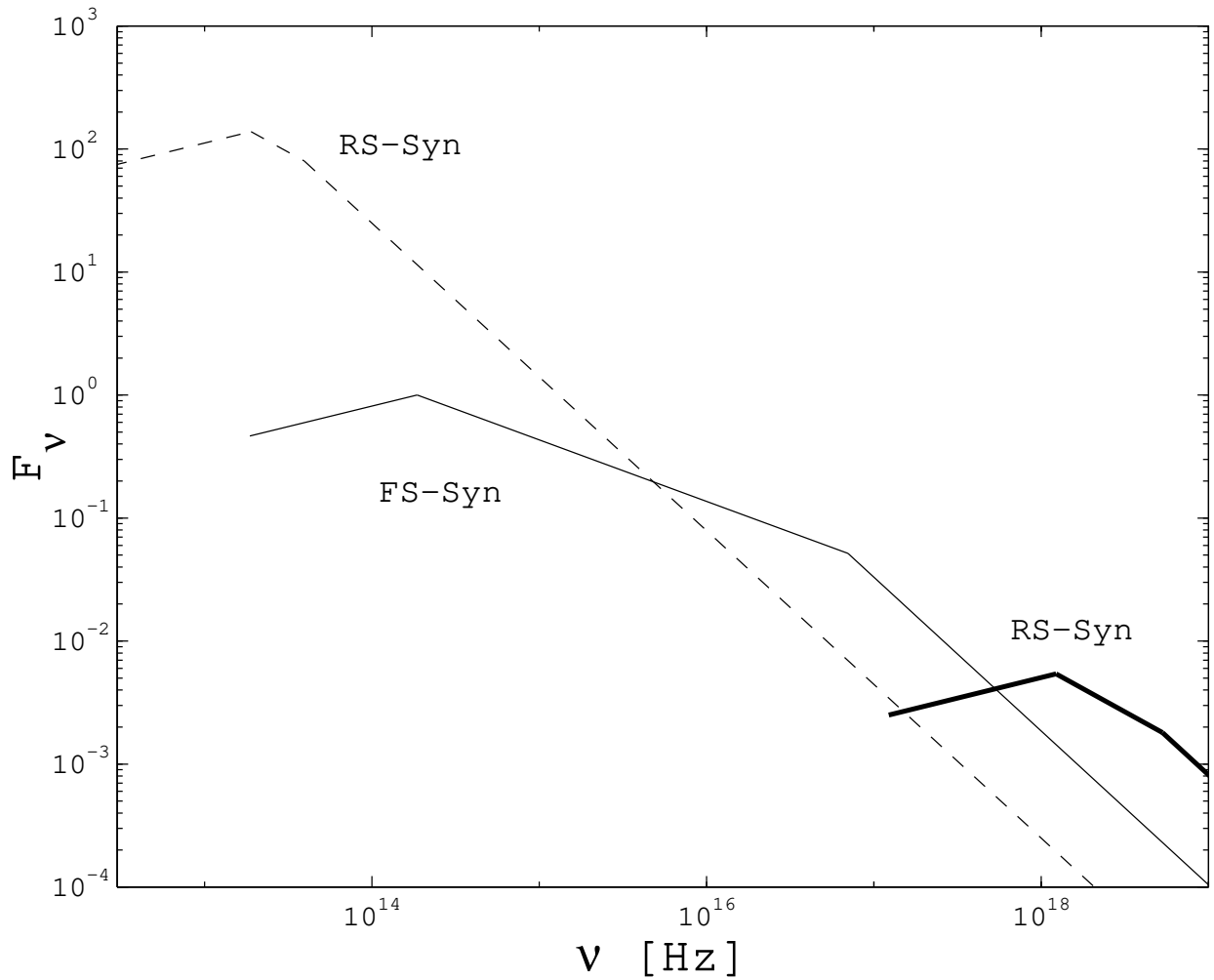


Fig. 1.— Spectrum at the deceleration time: Reverse Shock SSC (thick solid) and Synchrotron (thin dashed) emission, and Forward Shock Synchrotron emission (thin solid). $z = 1, E_{52} = 1, \Gamma_0 = 80, n = 5, \epsilon_e = 0.3, \epsilon_B = 0.03$ and $\epsilon_{B,f} = 0.01$ The flux is normalized at the forward shock peak.

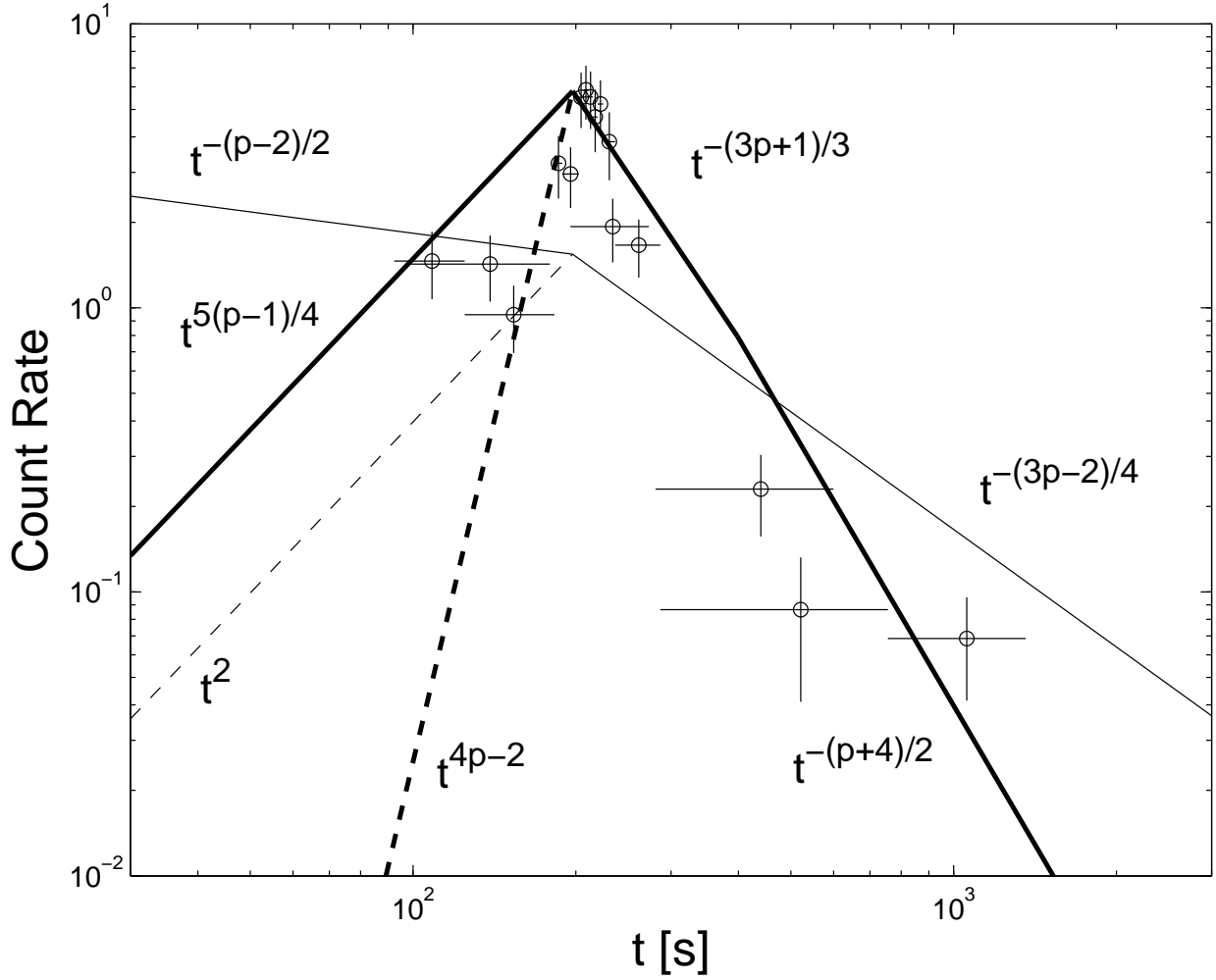


Fig. 2.— X-ray Light Curve: Reverse Shock SSC (thick solid) and Forward Shock Synchrotron emission (thin solid). The parameters are the same as in figure 1 except $\Gamma_0 = 79$. The circles represent the X-ray light curve (counts s^{-1}) of GRB 050406 from Romano et al. (2006). The theoretical light curves are normalized as the reverse shock SSC emission at the deceleration time fits the observed peak (the peak counts ~ 6 counts s^{-1}). If the width of the fireball shell is constant before the deceleration, the shock emissions rise more rapidly at the beginning (dashed lines).

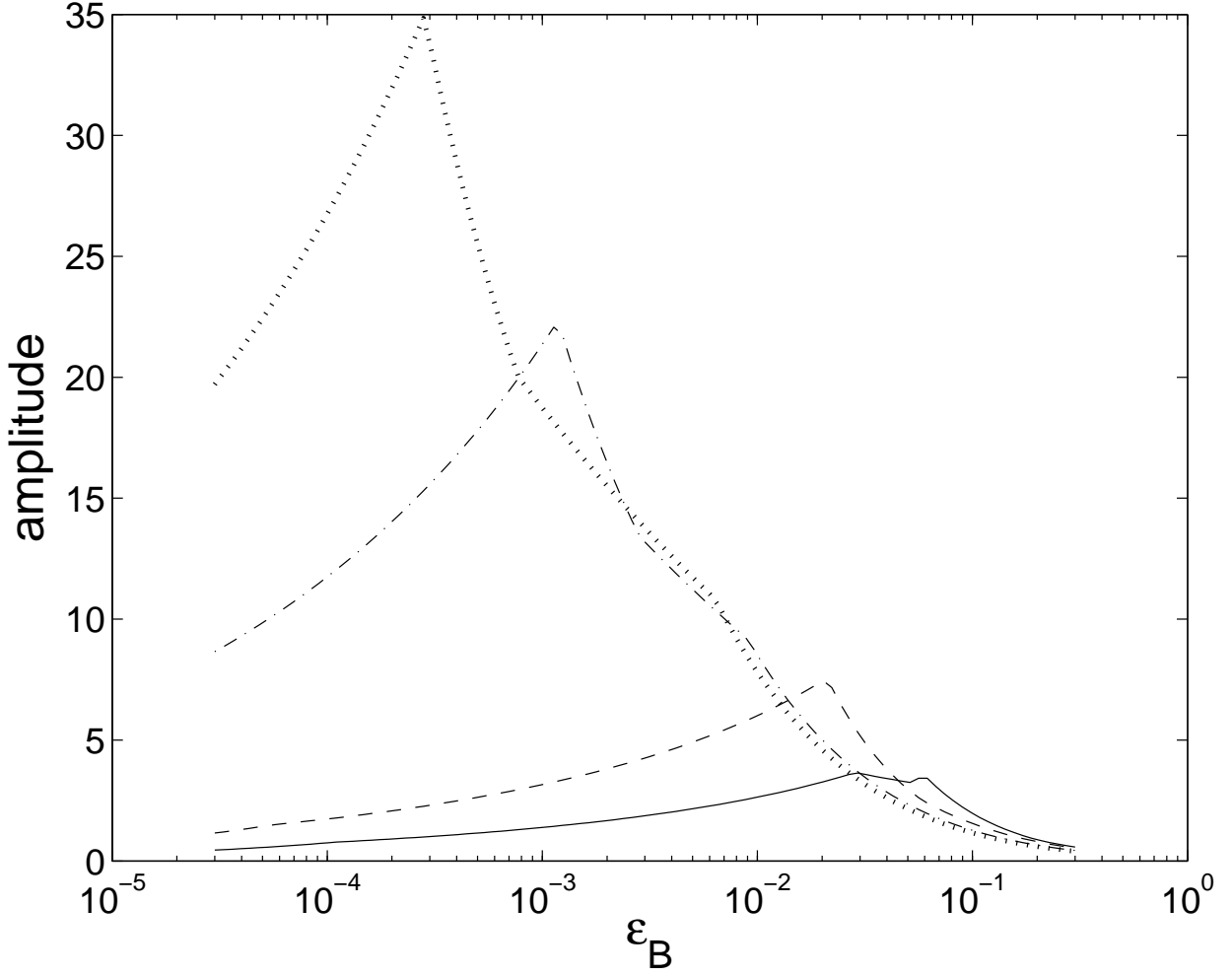


Fig. 3.— X-ray flare amplitude: Flux ratio between the reverse shock IC and forward shock synchrotron emission $F_\nu^{IC}/F_{\nu,f}$ at X-ray band (5keV) at the deceleration time is plotted as a function of ϵ_B . $n = 5$ (solid), 10 (dashed), 50 (dashed dotted) or 100 (dotted). $z = 1$, $E_{52} = 1$, $\epsilon_e = 0.3$ and $\epsilon_B/\epsilon_{B,f} = 3$. For a smaller ϵ_B , the Compton parameter x is larger and the typical frequency of the IC emission ν_m^{IC} is lower. The amplitude of an X-ray flare peaks at a moderate ϵ_B with which ν_m^{IC} is close to the X-ray band.